Available online at www.sciencedirect.com

SciVerse ScienceDirect

Ceramics International 39 (2013) 3279–3292

CERAMICS INTERNATIONAL

www.elsevier.com/locate/ceramint

Preparation of WC–W_2C composites by arc plasma melting and their characterisations

T. Dash, B.B. Nayak*

CSIR-Institute of Minerals and Materials Technology, Bhubaneswar-751013, India

Received 11 August 2012; received in revised form 26 September 2012; accepted 4 October 2012
Available online 23 October 2012

Abstract

WC–W_2C composites of seven different compositions (in the range of 30–50 at% C) have been prepared by arc plasma melting and in situ cooling. Microstructural characterisations of the melt-cast composites done by X-ray diffraction, transmission electron microscopy, selected area electron diffraction, field emission scanning electron microscopy and energy dispersive spectroscopy (of X-ray) identify the various phases that grow in the composites consisting of WC, W_2C and unbound C (graphite and diamond/ diamond like carbon); and the grains are seen to develop three types of contrast, such as white, grey and dark, depending on degree of carbon content. While the white grains show marginal higher microhardness than the grey ones, the dark grains show the lowest microhardness. Nanoindentation technique exhibited 31–54% higher microhardness value compared to microindentation technique. Young's moduli determined by nanoindentation technique show values in the range 514–754 GPa indicating reduced brittleness of the composites. Micro Raman spectra recorded on the grey and the white grains identify presence of several molecular phases: WC (major), WC–O and W═O (minor). Raman peaks of C due to G, 2G, D, D′, 2D, G+D, T, T+D phases are also detected in various grains. It is found that W_2C phase in the composites is not Raman active (incident with 514 nm Ar^+ radiation). Overall effort has been made in the work to correlate carbon content with various microstructural properties and hardness.
© 2012 Elsevier Ltd and Techna Group S.r.l. All rights reserved.

Keywords: B. Composites; Arc plasma; Microhardness; Tungsten carbide

1. Introduction

Tungsten carbide (WC) is an important hard compound that finds wide use in cutting tools, wear resistance components and hard facing applications. Carbon reacts with tungsten to produce compounds like WC, α-WC_{1-x} and W_2C. While WC_{1-x} is metastable, WC and W_2C are the two stable phases. WC, the mono carbide of tungsten, shows superior properties like high melting point (~2750 °C), high hardness (16–22 GPa) and high fracture toughness (28 MPa $m^{1/2}$ when bonded with Co) [1–3]. It is also characterised by very high compressive strength (5 GPa at 20 °C) and high corrosion resistance [4–6]. W_2C is the semi/sub carbide of tungsten which is variously reported to exhibit lower [7,8] as well as higher [9–11] hardness than WC. Because of the high melting point and the brittle nature of tungsten carbide, metals like Co, Ni and Fe are usually added to it for binding to form cemented carbide cutting tool tips [12–15]. Binder increases toughness and prevents brittle fracture in sintered cemented carbide tool tips but results in degradation of the corrosion and oxidation resistance. The application lists of tungsten carbide include critical components such as spray injection nozzle, sand blasting nozzle, guide sleeve in machines, thread guide in textile industry, micrometre anvil, burnishing tool, centre for lathe and grinder, ball point tip, teeth and jaw of excavator and rock cutting drill bit, etc. In rock cutting and hard facing applications, it is widely observed that WC–W_2C composite shows better performance than pure WC. Of late, tungsten carbide has drawn the attention of nuclear materials scientists due to its high neutron absorption coefficient [16]. Its performance in neutron shielding is better than the conventional materials

*Corresponding author. Tel.: +91 9238304338; fax: +91 0674 2581637.
E-mail addresses: bbnayak@immt.res.in, bijan_nayak@yahoo.com (B.B. Nayak).

0272-8842/$ - see front matter © 2012 Elsevier Ltd and Techna Group S.r.l. All rights reserved.
http://dx.doi.org/10.1016/j.ceramint.2012.10.016

like SS 316LN used in plasma based fusion reactors like tokamaks.

Tungsten carbide components are generally fabricated by powder metallurgy process or by melt-casting. While the powder metallurgy process involves a number of process steps such as mixing with binder, compaction, sintering, etc., melt-casting of tungsten carbide into desired shape and size is less cumbersome and easy to adapt in industrial practice. Melt-cast components show lower porosity compared to sintered products. In view of high melting point of tungsten carbide, induction furnace and graphite furnace are used in industries to melt this compound [17,18]. Both the heating processes are costly and energy intensive. Thermal arc plasma (operating in transferred arc mode) offers a viable alternative to induction and graphite furnaces due to several advantages in high temperature melting [19,20] and therefore chosen here for preparation of melt-cast WC–W_2C composites.

WC–W_2C composites of seven different compositions (30–50 at% C) have been prepared by arc plasma melting method and their microstructural and mechanical properties have been evaluated using X-ray diffraction (XRD), transmission electron microscopy (TEM), selected area electron diffraction (SAED), field effect scanning electron microscopy (FESEM), energy dispersive spectra (EDS) of X-ray, micro and nanoindention techniques and micro Raman spectroscopy. The paper makes an effort to correlate properties of the melt-cast composite such as phase, microstructure, microhardness, etc. with composition, particularly the C content. For the first time, the paper reports the significant improvements in microhardness values (more than 30%) of tungsten carbide grains when determined by nanoindentation technique and establishes the non-Raman active property of W_2C.

2. Experimental

WC and W taken in the form of powder were mixed at seven different ratios between 0 and 55.5 wt% of W (Table 1) to prepare respective homogenous mixtures at 0.1 kg scale. Corresponding C composition was varied between 50 and 30 at%. Specifications of the starting powder procured from M/s Rapicut Carbides Ltd., India are as follows:

W powder: *grain size* 4–5 μm
WC powder: *grain size* 4–7 μm
C wt% in WC: 6.11–6.16 (*bound* C), 0.05 max (*free* C)

2% polyvinyl alcohol (PVA) solution (in water) was used as binder for pelletizing the powders under uniaxial compaction by applying a load of 4.5 T (pressure: 140.44 MPa) for 30 s. After compaction, the green pellets were air-dried for 3 to 4 h to develop good handling strength. The air-dried pellets were melted in a 30 kW extended arc plasma furnace using graphite crucible. Following arc conditions were maintained during melting: voltage 45–60 V (dc) and current 300–350 A. Ar was used as plasma forming gas and it was introduced into the reactor through an axial hole in the graphite cathode (top electrode) at a rate of 1.5 l per min. As WC is a good conductor of electricity, positive polarity of arc was maintained on the charge (WC + W pellet) through contact with the graphite crucible, thus facilitating production of transferred-arc condition which transfers more energy to charge in the melting process. The top graphite electrode (in the form of a circular rod) was connected to negative polarity of power supply and served as the cathode. At the beginning, the top cathode was brought to close proximity of the charge (pellet) kept on the inner base of crucible by employing rack and pinion arrangement and then the arc was initiated by switching on the electric power. The cathode was then slowly withdrawn up to a distance of 0.03–0.04 m in the vertical upward direction. Plasma (Ar) was thus formed and got stabilized at an arc length of around 0.035 m. The details of the arc plasma furnace melting have been reported in the earlier works [19–21]. It took 25–40 min to completely melt the charge depending on the mass of the pellets. Then, the liquid melt was allowed to solidify/ cast in situ within the graphite crucible by switching off power in the arc and allowing furnace

Table 1
Variation of W, WC and C composition in the charge (pellet) vis-à-vis electrical energy consumption recorded in arc plasma melting and recovery/yield of WC–W_2C composite products.

Sample ID	Wt% in charge stage*			at% of C in charge stage (theor. calc.)	Total wt% of C in melt-cast sample (expt. detnd.)	Electrical energy consump. recorded for arc plasma melting (kWh/0.1 kg)	Recovery/ yield of WC–W_2C product from furnace (wt%)
	W taken	WC taken	C (theor. calc.)				
WC-1	0	100	6.14	50.0	6.27	13.9	91.1
WC-2	5	95.0	5.83	48.6	5.76	13.5	85.0
WC-3	16	84.0	5.15	45.4	4.88	15.7	86.5
WC-4	32	68.0	4.17	40.0	4.34	15.0	89.2
WC-5	37.2	62.8	3.85	38.0	3.69	11.0	91.4
WC-6	48.3	51.7	3.17	33.4	3.07	15.0	86.0
WC-7	55.5	44.5	2.72	30.0	3.15	11.4	83.6

*Atomic weight values were taken as: W = 183.84, C = 12.02.

cooling. Ar flow at a rate of 0.5 l/min was continued for 1 h in the furnace during cooling to prevent oxidation of the cast product. After 4–5 h of furnace cooling, the cast product attained room temperature and was then taken out for various characterisations.

XRD analysis of the cast composites was done using powder samples in the 2θ range 5–95° at a scan speed of 0.017 min^{-1}. Mirror polished samples prepared by grinding and fine polishing (by diamond paste) were used for FESEM, EDS (of X-ray), micro and nano indentations. Micro Raman spectra studies were carried out with powder samples. The following analytical instruments were used in the evaluation of microstructural and mechanical properties: XRD-PANalytical X'Pert Pro diffractometer with CuKα radiation ($\lambda = 0.15406$ nm), TEM—TECNAI G^2 (200 kV), FEI, Netherland, with facility for SAED and Gatan Inc.'s digital micrograph^{TM} software for the phase and plane identifications, FESEM-ZEISS SUPRA 55 (back scattered mode) (with above Gatan software), EDS-Oxford, X-Max (20 kV accelerating potential) attached to FESEM, Microhardness tester – LECO (load 0.5 kg, 13 s dwell time), Nanoindenter—UMIS system (Fisher-Cripps, Australia) with diamond Berkovich indenter (tip diameter: 400 nm) at a maximum applied load of 50 mN, Micro Raman spectrometer–Renishaw inVia Reflex (UK) with a spectral resolution of 1 cm^{-1}(Ar^+ laser, $\lambda = 514$ nm). Using the Oliver-Pharr method [22], the load depth data were analysed to determine Young's moduli of the samples. For calculation purpose, Poisson's ratio of the tungsten carbide composite was taken 0.21 which is the typical value for WC [23].

3. Results and discussion

3.1. WC–W_2C composites preparation

In industrial practice, it is generally observed that when WC undergoes solidification or casting (in inert atmosphere) after melting, the single phase WC does not grow again but it grows along with W_2C. The melt-cast product is a composite of WC–W_2C which exhibits higher hardness than WC [17]. WC–W_2C composite is commercially known as fused tungsten carbide and is mostly used in making drill bits for oil well digging, rock cutting and RCC (reinforced concrete cement) cutting. The phase diagram of W–C system shown in Fig. 1 is widely referred in literature [24–25]. Phase diagrams are worked out on the basis of thermodynamic equilibrium reaction/process. In contrast, our results have been obtained on the basis of a non-equilibrium plasma process. In absence of any report in literature on non-equilibrium growth process of WC–W_2C composite, an effort has been made here to understand our results with reference to above phase diagram in Fig. 1. It may be marked in the figure that the composite WC–W_2C grows by eutectoid transformation (including hypo- and hyper-eutectoid) at 2380 °C between 33.4 and 50 at% C. The growth of single W_2C phase in the narrow

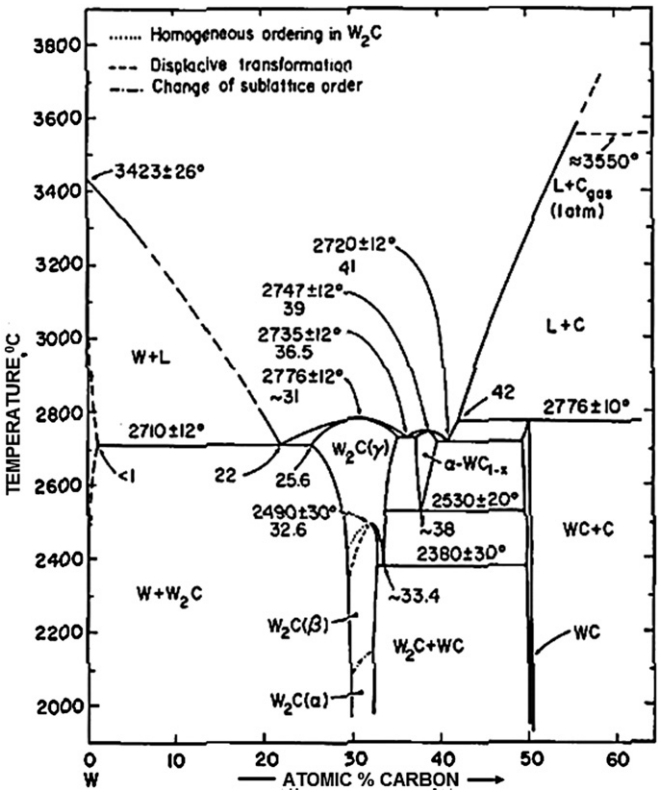

Fig. 1. Phase diagram of W–C system (Refs. [24,25]).

range 30–33.4 at% C is difficult to achieve due to C loss taking place during melting and also owing to possibility of unwanted (eroded) C addition from graphite crucible during melting operation. Keeping such points in view, we have chosen here the variation of C in the W–C system in the range of 30–50 at% (at seven different values) and made a systematic study to evaluate the microstructural and mechanical properties of the resulting WC–W_2C cast composites developed by the non-equilibrium melting process (such as plasma) and correlate composition in terms of C content/W:C ratio with product recovery/yield, energy consumption (electrical), phases of tungsten carbide and carbon, microstructure, microhardness and molecular peaks in Raman spectra. So far no one seems to have reported such kind of detailed study of the composites produced by the plasma method. Because of brittle nature of tungsten carbide, no cold working of the casts was possible. The high melting point (~2750 °C) of WC makes it difficult for post casting heat treatment; therefore the as-cast samples were directly characterised. The proportion of W in the starting mixture of WC+W (each taken in its powder form) was varied to change the W/C ratio in the composite. The C% (Table 1) and the W:C ratio (Table 2) have been used in this work to identify/index each composite towards correlation with other properties. It is marked that white, grey and dark contrast of the grains in FESEM micrographs (Fig. 2) occur due to the presence of different amounts or quantities of C and their distributions

Table 2
Lattice constants (in nm) determined from XRD for arc plasma melt-cast (WC–W_2C) composites.

Sample ID (ratio in at%)	WC phase (hexagonal structure)	W_2C phase (hexagonal structure)	C phase (hexagonal structure)
WC-1 (W:C=50:50)	a=0.2913, c=0.2849	a=0.5195, c=0.4744	a=0.246, c=0.6729
WC-2 (W:C=51.4: 48.6)	a=0.2912, c=0.2844	a=0.519, c=0.4737	a=0.246, c=0.6727
WC-3 (W:C=54.6: 45.4)	a=0.2904, c=0.2836	a=0.5195, c=0.472	a=0.246, c=0.6729
WC-4 (W:C=60: 40)	a=0.2912, c=0.2843	a=0.5193, c=0.4739	a=0.246, c=0.6724
WC-5 (W:C=62:38)	a=0.2916, c=0.2847	a=0.5195, c=0.474	a=0.246, c=0.673
WC-6 (W:C=66.6:33.4)	a=0.291, c=0.284	a=0.5195, c=0.473	a=0.246, c=0.6716
WC-7 (W:C=70:30)	a=0.2906, c=0.2836	a=0.5195, c=0.4725	a=0.246, c=0.6727

Standard values

Phase and structure	*Lattice constants (in nm)*	1999 *JCPDS file number*
WC (hexagonal)	a=0.2906, c=0.2837	73-0471
W_2C (hexagonal)	a=0.519, c=0.4724	79-0743
C (graphite) (hexagonal)	a=0.247, c=0.6724	41-1487

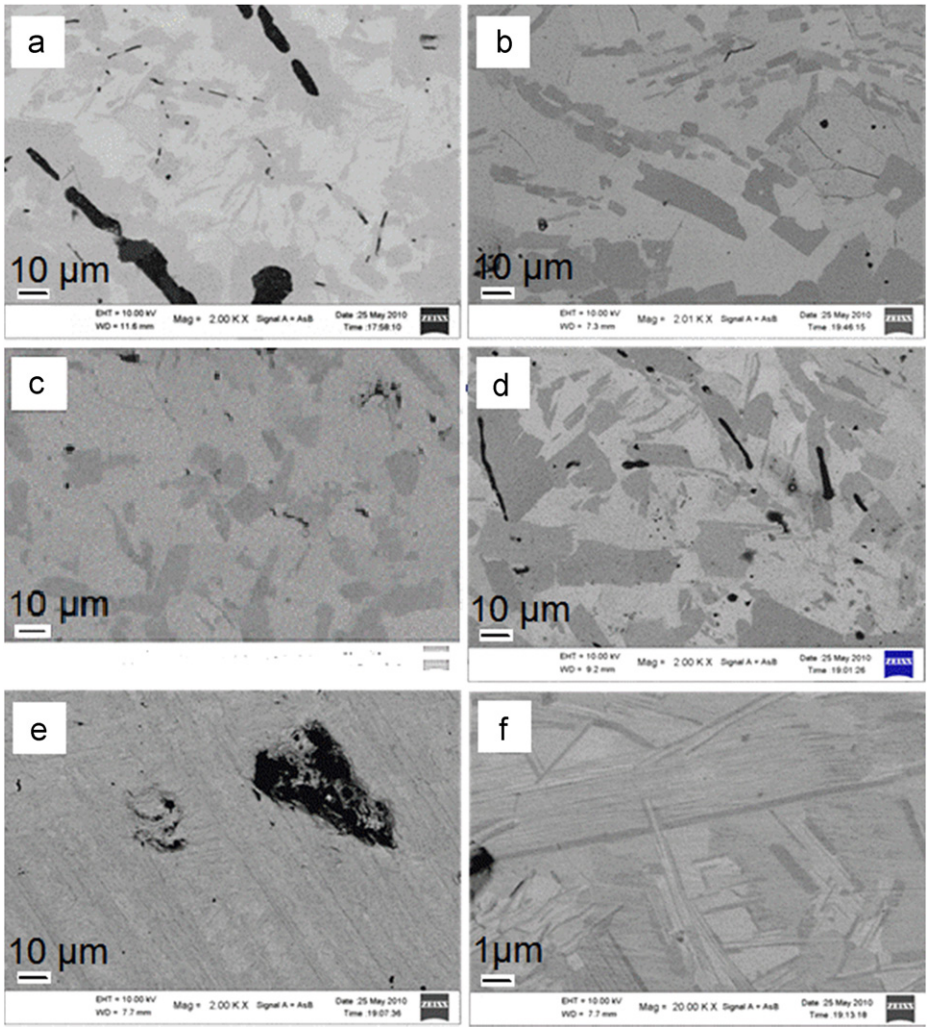

Fig. 2. FESEM micrographs of arc plasma melt-cast sample surfaces with different C contents: (a) WC-1 (50 at% C), (b) WC-3 (45.4 at% C), (c) WC-5 (38 at% C), (d) WC-6 (33.4 at% C), (e) WC-7 (30 at% C) and (f) WC-7 (30 at% C).

(determined by area fractions in micrographs) (Table 4) can serve as indices to calibrate the composites. The details of the distributions are discussed in subsequent Section (3.4) dealing with microscopy and microhardness.

3.2. Energy consumption and product yield

Variation of power consumption in the arc plasma melting for preparation of WC–W_2C composites of seven

different compositions along with product recoveries/ yields are shown in Table 1. At charge stage, mixing of W and WC powder was done in the following ranges: W 55.5–0 wt% and WC 44.5–100 wt%. The total C content variation in the composites (determined by calculation) occurs in the range of 2.72–6.14 wt% (30–50 at% C), where as experimentally it was found in 3.15–6.27 wt% range. Electrical energy consumption for melt-casting of the WC–W_2C composites is found to be relatively high, i.e. 11–15.7 kWh/ 0.1 kg (110–157 kWh/ kg), which is around 30 times higher than that of iron. Such high figure may be attributed to high melting point of WC and energy loss (20–25% of heat energy) taking place in a semi-open type 30 kW dc-arc plasma furnace employed in this work in the laboratory scale investigation. Recovery or yield of the composite products from the furnace varies between 83.6 and 91.4 wt%. It is reasonably high and can be further improved upon beyond 90 wt% by suitably minimising heat loss. Excepting the case of pure WC, i.e. WC-1 sample(50 at% C), the recovery/yield is noticed to show an increasing trend from 48.6 at% C sample (WC-2) to 38 at% C sample (WC-5) and then the trend is reversed up to 30 at% C sample (WC-7). The highest yield of 91.4% for WC-5 sample (38 at% C) occurs for eutectic composition, the reason of which is not apparent at this stage.

3.3. XRD analysis of WC–W_2C composites and lattice constants

Various phases grown in the plasma melt cast composites were identified from their XRD patterns by comparing the observed *d* values with 1999 JCPDS data files (WC: 73-0471, W_2C: 79-0743, C (graphite-2H): 41-1487, C (diamond): 75-0410 and W: 04-0806). Fig. 3A shows only one phase, i.e. WC, in the starting tungsten carbide powder. XRD patterns of the melt-cast composites of seven different compositions, including melt-cast pure WC (sample WC-1), are presented in Fig. 3B. It is observed that all melt-cast products exhibit two major phases such as WC and W_2C. Occurrence of free C (graphite-2H) is significantly marked in two samples, viz. WC-6 (33.4 at% C) and WC-4 (40 at% C). In WC-5 (38 at% C), WC-3 (45.4 at% C) and WC-1(50 at% C), the free C (graphite) shows small peaks; and in the rest of the samples, i.e. WC-2 (48.6 at% C) and WC-7 (30 at% C); traces of the

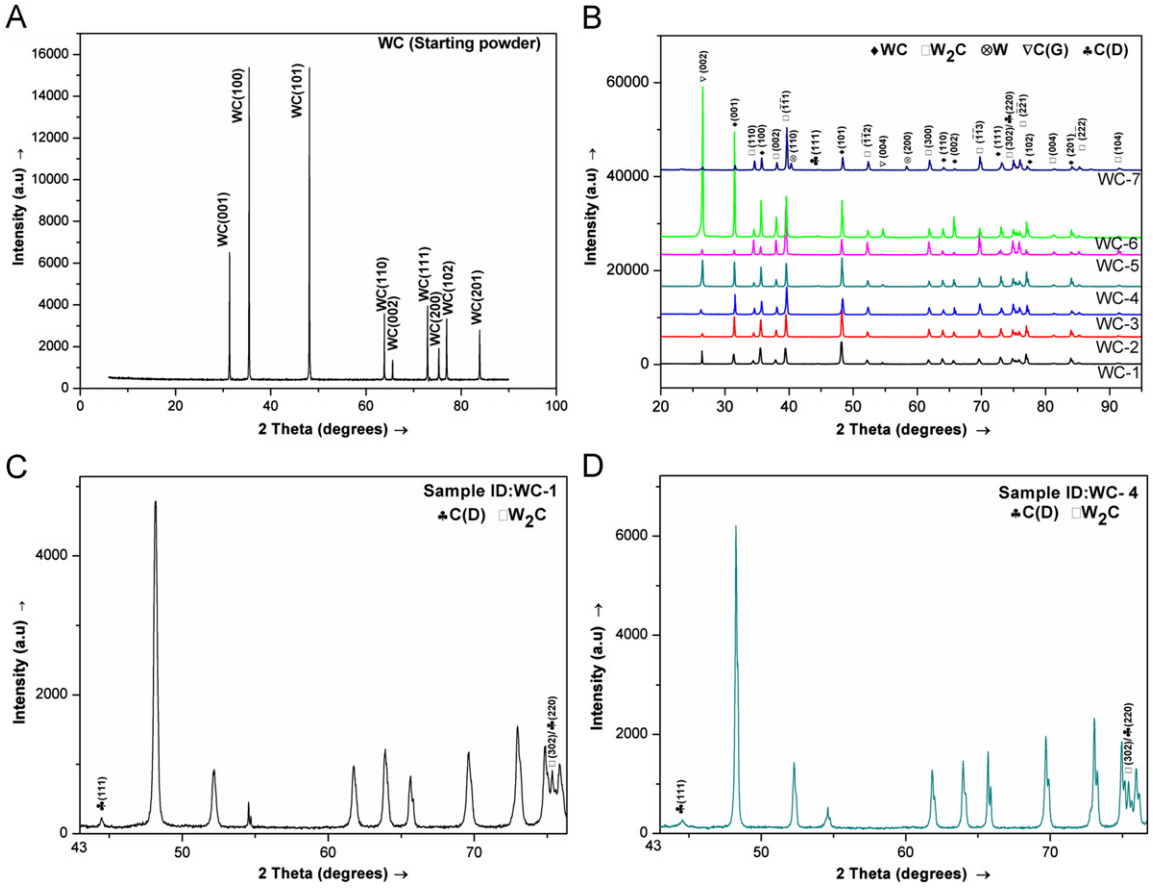

Fig. 3. (A) XRD pattern observed for starting tungsten carbide powder. (B) XRD patterns observed for arc plasma melt-cast tungsten carbide composite samples at different W to C ratios (detailed ratios are shown in Table 2); Symbol C(G) stands for graphite phase, C(D) stands for diamond/DLC phase. (C) XRD pattern of arc plasma melt-cast sample WC-1 depicting small peaks due to diamond/DLC/W_2C. (D) XRD pattern of arc plasma melt-cast sample WC-4 depicting small peaks due to diamond/DLC/W_2C.

free C (graphite) peaks are noticed. Quite small peak of C in diamond/DLC phase, denoted as C(D), appearing at around $2\theta = 44.58^\circ$, is observed in the respective diffractograms of WC-1, WC-4, WC-5, WC-6 and WC-7. Fig. 3C and D clarifies the small C(D) peaks of WC-1 and WC-4 samples. Moreover, the peak at around $2\theta = 75.53^\circ$ is found in all samples which may be attributed to C(D)/ W_2C. Trace of free W (metal) peak is observed only in the case of WC-7 (30 at% C) sample which may be due to some unreacted W, resulting at higher W/WC ratio in the charge stage. Also, possibility of dissociation/decomposition reaction taking place in tungsten carbide at 1250–1300 °C ($W_2C \Leftrightarrow (W) + WC$ [26]) cannot be ruled out to contribute to the presence of W metal. While WC is the only phase detected in the XRD of the starting tungsten carbide powder, the melt-cast sample of this powder (sample WC-1) shows extra phases such as W_2C and C (both graphite and diamond/DLC). Growth of C in different phases is also marked in different composition samples prepared in this work. Based on these observations, one may infer that the melt-cast products consist of WC–W_2C composite along with unbound C occurring in diamond/DLC and graphite phases. The total C (bound with W + free/unbound) content for each composite is seen to vary for all cases of the seven samples. Experimentally determined values in melt-cast samples vis-à-vis calculated values of C (total content) in respective samples (at charge stage) are compared in Table 1.

C% in the WC–W_2C composites has been varied from 50 at% (6.14 wt%) to 30 at% (2.72 wt%) (Table 1). One may note from Fig. 3B that except two cases, i.e. WC-5 (C: 38 at%/3.85 wt%) and WC-7 (C:30 at%/2.72 wt%), in all other cases the major phase WC (0 0 1) shows improvement in peak intensity with decrease in C%. W_2C ($\bar{1}\bar{1}1$) (another major phase), shows increase in peak intensity with decrease in C% up to 38 at% (or 3.85 wt%) and then exhibits marginal change. It is also marked that except for the samples WC-2, WC-3, WC-5 and WC-7, the peak intensity of C (002) increases with decreasing in C%. Improvement of peak intensity is generally understood in terms of better crystallisation and increase in quantity/amount of phase occurring in any sample. The most intense peak due to C(D) (220)/W_2C (302) occurs in WC-5 sample which shows the lowest intense peak of graphite. It is observed that rest of the samples (except WC-5) having very low intense peaks of C (D) (220)/W_2C (302), do not show any significant trend. In non-equilibrium process like plasma melting, this kind of result is not unusual because of existence of varying temperature zones in the plasma region causing different reaction kinetics.

By using special software (Search test programme), the crystal structures of WC, W_2C and C are found to be hexagonal and cubic for W. The lattice constants of WC, W_2C and C (graphite) have been determined by using the d values of seven different samples determined from XRD in the above software (Table 2). These lattice constants are observed to closely match with that of the respective standard values in 1999 JCPDS data files. Lattice constants variations (maximum values) with respect to standard values are found as follows- WC: $a = 0.344\%$, $c = 0.422\%$ (increased); W_2C: $a = 0.096\%$, $c = 0.423\%$ (increased); C (graphite-2H): $a = 0.405\%$ (decreased), $c = 0.089\%$ (increased). The above marginal variations in lattice constants occur due to the difference in crystallisation phenomena taking place under different preparation methods. It may be worthwhile to mention that WC crystallises in hexagonal lattice with $P\bar{6}m2$ (187) space group, W_2C crystallises in hexagonal lattice with $P\bar{3}1m$ (162) space group and C crystallising in graphite phase grows in hexagonal lattice (2H polytype) with $P6_3/mmc$ (194) space group.

3.4. Microstructure and microhardness studies

Microstructures of all the arc plasma melt-cast samples were studied under FESEM where typical multiphasic morphologies are observed (Fig. 2). Lamellar structures were observed in Fig. 2e and f for WC-7 sample. Similar microstructure has been observed by Kublii and Velikanova [24] for arc furnace melted and quenched W–C samples containing 34–37 at% C. In other samples (WC-1 to WC-6), multiphasic granular microstructures are observed in the hypo- and hyper-eutectoid compositions. Grains of three types of contrast, such as white, grey and dark, are seen in the microstructures. Average grain sizes of the grey grains, measured from the FESEM micrographs, are presented in Table 3. The grain size is seen to vary from 2.8 to 11.8 μm. Fig. 4 shows EDS results of a typical sample WC-5 (38 at% C). While the dark grain (Fig. 4f) contains the highest amount of C (12.08 wt%), the white grain (Fig. 4d) contains the lowest C (3.07 wt%), and the grey grain (Fig. 4b) shows an in between C value (5.66 wt%). The dark grain contains C quantity around four times more than that of the white. SAED pattern of pure WC sample (starting powder) at a selected area is shown in Fig. 5. Fig. 6 records the SAED of melt cast WC-7 (30 at% C) sample taken on the white, grey and dark grains along with identification of planes due to different phases. The SAED pattern shown in Fig. 5b depicts the presence of WC and very weak spot due to W. This corroborates our finding in the XRD pattern depicting presence of WC only (Fig. 3A). Since XRD is not sensitive to detect very small (~0.1 wt%) or trace amount of any phase (like W here), such peak is found to be missing in Fig. 3A. It is evident from the SAED shown in Fig. 6b for sample WC-7 that the white grain identified in Fig. 6a (cirle1) constitutes of WC and W_2C intermix (containing more reflections of W_2C), and also existence of minor or trace amount of C in the diamond/DLC phase (C(D)) may not be ruled out in this. The semi-white or grey grain identified in Fig. 6a (circle 2) shows intermix of WC and W_2C (containing more reflections of WC) in the SAED pattern (Fig. 6d) without showing any trace of carbon. Fig. 6a (circle 3)

identifies a dark grain under selection and records its SAED pattern as shown in Fig. 6c. The dark grain constitutes of WC and W_2C as major phases (containing more reflections of WC) and presence of carbon is significant here because two spotted rings of C (graphite) are marked. Thus, it may be concluded that the dark appearance/contrast of any grain in

Table 3
Microhardness and grain size determined for the arc plasma melt-cast (WC–W_2C) composites.

Sample ID	Hardness ($VHN_{0.5}$) determined by the micro indentation method			Average grain size in grey phase, determined from FESEM (in μm)
	White grain	Grey grain	Dark grain	
WC-1 (C: 50 at%)	1708 ± 70	1670 ± 60	616 ± 20	8.6
WC-2 (C: 48.6 at%)	1714 ± 30	1686 ± 40	529 ± 12	8.4
WC-3 (C: 45.4 at%)	1790 ± 60	1774 ± 50	660 ± 6	8.5
WC-4 (C: 40 at%)	1780 ± 58	1770 ± 30	535 ± 12	11.8
WC-5 (C: 38 at%)	1890 ± 48	1818 ± 40	646 ± 10	9.8
WC-6 (C: 33.4 at%)	1684 ± 60	1604 ± 58	589 ± 30	11.6
WC-7 (C: 30 at%)	2080 ± 20	2055 ± 25	516 ± 15	2.8

Table 4
Distribution of white, grey and dark areas/grains determined from FESEM microstructures of arc plasma melt-cast WC–W_2C composites.

Sample ID	Fig. no	% of white area/grain	% of grey area/grain	% of dark area/grain
WC-1 (C: 50 at%)	2a	32.836	61.860	5.304
WC-3 (C: 45.4 at%)	2b	67.135	31.575	1.290
WC-5 (C: 38 at%)	2c	70.077	28.952	0.971
WC-6 (C: 33.4 at%)	2d	60.324	35.169	4.507

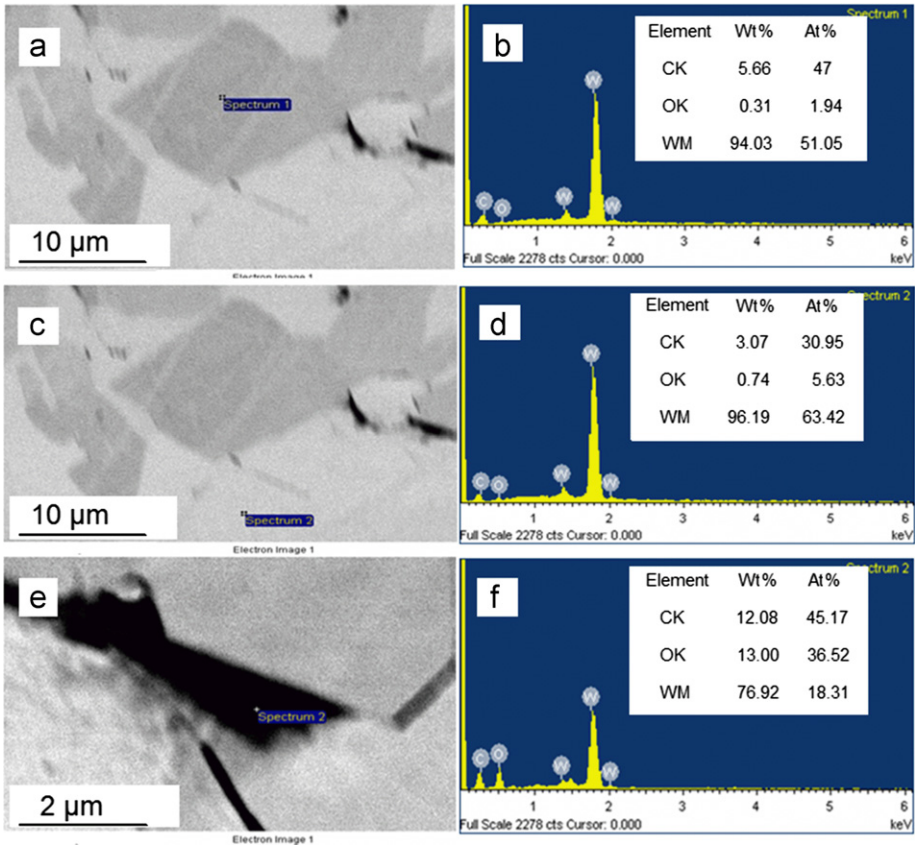

Fig. 4. EDS analysis of arc plasma melt-cast sample WC-5 (38 at% C) recorded on three types of grains/phases (image in BSE mode): grey (a & b), white(c & d) and dark (e & f).

the melt-cast sample occurs due to presence of relatively more amount of carbon in graphite form.

Amount/quantity of white, grey and dark grains/phases (in micrograph), present in each of the four samples (WC-1, WC-3, WC-5 and WC-6) has been calculated (in %) from respective area fraction (out of the total area in the micrograph) that each grain occupies in micrographs (Fig. 2(a–d)). Table 4 shows the distributions of various grains/phases and their corresponding trends with decreasing C% in the WC–W_2C composites. It is observed that up to 38 at% C (sample WC-5); the amount of white grain in the composites increases with decrease in C% and beyond this limit it shows a trend reversal. In the case of grey grain, a trend opposite to that of white grain is marked. Dark grain containing more graphite shows lowest area fractions in the micrographs and it is marked that its amount decreases with

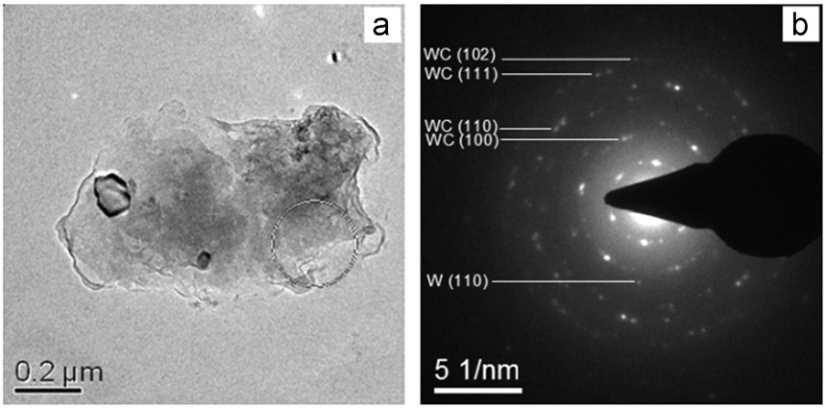

Fig. 5. TEM microstructure and SAED of the starting WC powder: (a) microstructure observed in WC grain and (b) SAED observed in the selected area (within the circle) shown in (a).

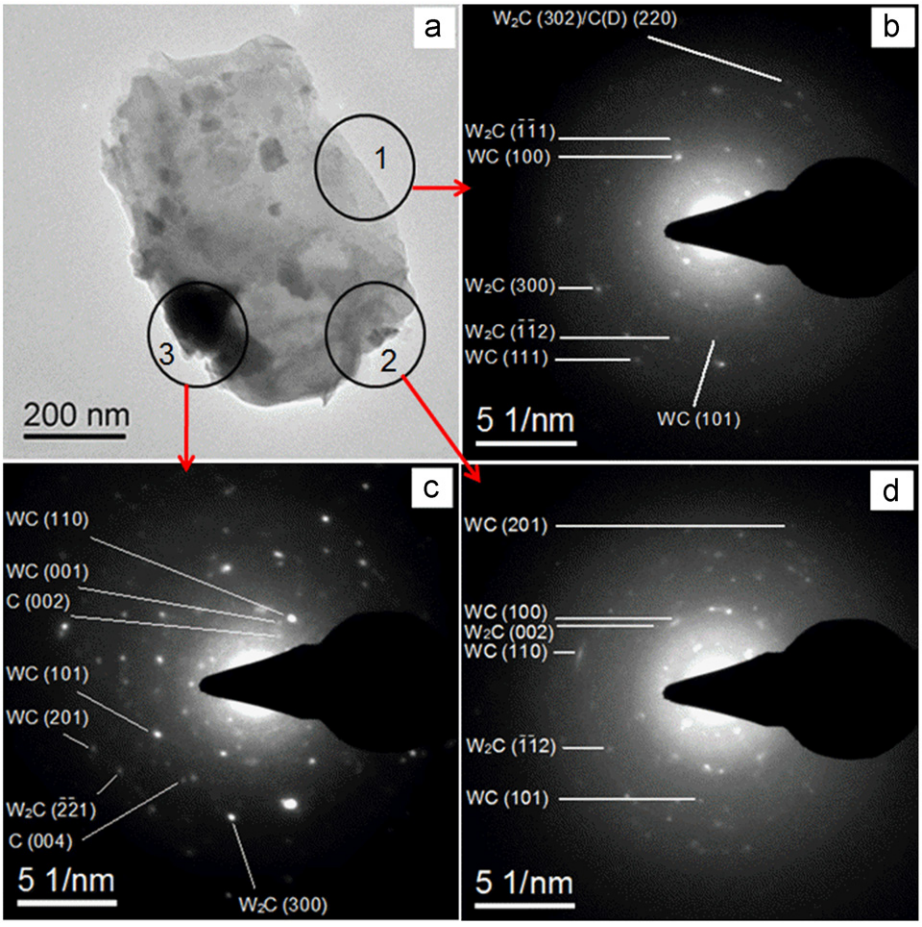

Fig. 6. TEM observations in arc plasma melt-cast sample WC-7: (a) TEM microstructure, (b) SAED taken on the selected white area/phase (circle 1), (c) SAED taken on the dark area/phase (circle 3), and (d) SAED taken on the semi-white/grey area/phase (circle 2).

decrease in C% up to 38 at% C, and beyond this a reverse trend occurs. The above irregular distribution trend of grains could be attributed to non-equilibrium reaction kinetics taking place in the plasma melt-casting operation.

Fig. 7 presents some typical optical micrographs showing Vickers indentation marks (microindenter) (0.5 kg load) on the white and grey grains/areas of WC-3 (45.4 at% C), WC-5(38 at% C) and WC-7(30 at% C) samples. Microhardness was calculated from the indentation technique by the formula [27].

$$\mathrm{VHN} = 1.8544\ \mathrm{P}/d^2 \quad (1)$$

where P is the applied load and d is the average length of diagonals.

No cracks are noticed on the surface, thus suggesting that the melt-cast carbides do not exhibit brittle behaviour at a load of 0.5 kg. Experimentally determined microhardness values of white, grey and dark grains for all samples are presented in Table 3. Microhardness of the white grains occurs in the range 1684–2080 $VHN_{0.5}$ as against 1604–2055 $VHN_{0.5}$ for the grey grains, thus showing a little higher hardness for the white grains. The marginal improved hardness of white grain may be due to the presence of C (D) and T (sp^3 bonded carbon, peak identified from Raman spectra as discussed below), and occurrence of more amount of W_2C phase, as seen from SAED (Fig. 6b). The W_2C attribution may not be out of place because recent literatures [9–11] cite higher hardness of W_2C compared to WC. Fig. 8 shows plot of microhardness variation with C% and W% in the melt-cast samples. The highest hardness value (2080 ± 20 $VHN_{0.5}$) is marked in the white grain of the sample WC-7 (70 at% W and 30 at% C). The dark grains exhibit hardness in the range of 516–660 $VHN_{0.5}$ which is around one third of the values shown by the white and grey grains. This implies the presence of higher amount of C (graphite) in dark grain. It corroborates our EDS (Fig. 4) and TEM (Fig. 6) results. Orban [28,29] had reported that W_2C/WC ratio and C% are the two major factors that influence the microhardness of quasi eutectoid mixture of tungsten carbide. In the present work, we have found that the eutectic sample WC-5 (38 at% C) shows the highest microhardness for both the white and the grey grains in the C composition range of 33.4–50 at%. In the eutectoid range (including hypo and hyper range), the

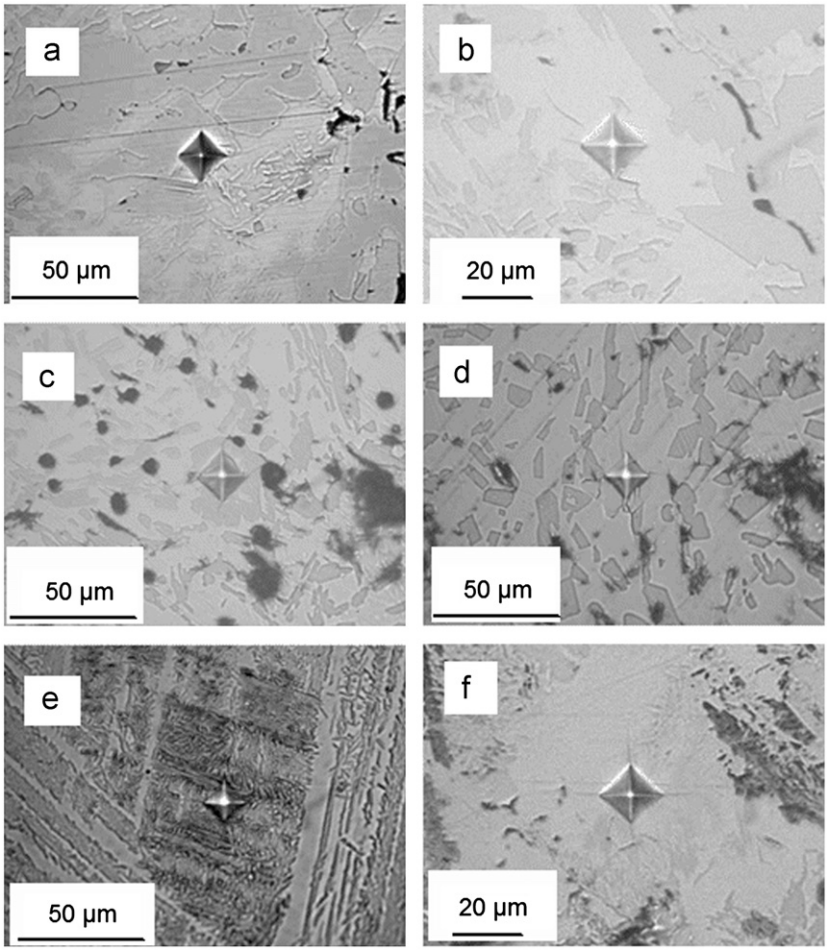

Fig. 7. Optical micrographs showing indentation marks made by diamond tip of Vickers microhardness tester on grey and white areas/grains of arc plasma melt-cast samples having different at% C in charge stage: (a) and (b) show indentation on grey and white area/phase of WC-3 (45.4 at% C) sample, (c) and (d) show indentation on grey and white area/phase of WC-5 (38 at% C) sample, (e) and (f) show indentation on grey and white area/phase of WC-7 (30 at% C) sample.

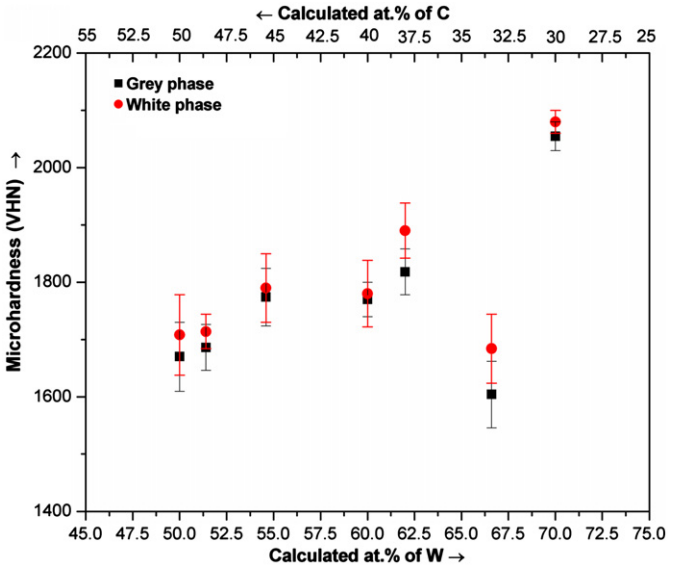

Fig. 8. Graph showing plot of microhardness vs. composition (C and W at%) in the grey and white areas/grains of the arc plasma melt-cast samples.

microhardness is found to increase with decrease in C content (up to 38 at% C), and below this composition it drops significantly at 33.4 at% C (Fig. 8). At 30 at% C, the microhardness is found to show respective highest values for white and grey grains. A dip in microhardness for 33.4 at% C sample (WC-6) is observed in Fig. 8 which may be explained on the basis of higher graphite content (marked in XRD pattern shown in Fig. 3B). The logic is further confirmed in case of 40 at% C sample (WC-4) and which appears in line with Orban's reasoning [28,29].

In microindentation method, the possibility of indenter tip falling on two different grains (at the same time) may not be ruled out due to relatively larger tip dimension. To overcome such an error, microhardness was determined by nanoindentation technique where it was ensured to mount the nanoindenter tip (400 nm diameter) on single grains during measurements. Microhardness of five samples with different compositions determined by the Nanoindentation method is presented in Table 5. Fig. 9 shows the typical nanoindentation marks on single grains at different grain-sites of WC-4 (40 at% C) sample. It is evident that inclusion of above mentioned possible error has thus been avoided. The Nanoindentation method exhibits significantly higher microhardness values (Table 5) for both white (2334–2765 VHN) as well as grey grains (2265–2615 VHN). The trend of marginal higher microhardness of white grain over that of grey grain is maintained as observed in Table 3. Microhardness values for white and grey grains of the five samples are found to increase by 36.172–49.55% and 31.397–54.488% respectively. For dark grains, microhardness decreases from 516–660 to 11–69 VHN. In Table 5 it is evident that in the composition range of 48.6–33.4 at% C, micro hardness is found to be the maximum for 38 at% C sample (WC-5, eutectic composition). Both the white as well as the grey grains

Table 5
Microhardnesses and Young's moduli of the arc plasma melt-cast WC–W_2C composites determined by the Nanoindentation method.

Sample ID	Microhardness (VHN)		Young's modulus (GPa)	
	White grain	Grey grain	White grain	Grey grain
WC-2 (C: 48.6 at%)	2334 ± 51	2265 ± 59	558 ± 12	754 ± 50
WC-3 (C: 45.4 at%)	2448 ± 67	2331 ± 82	561 ± 51	728 ± 61
WC-4 (C: 40 at%)	2662 ± 39	2513 ± 17	526 ± 50	601 ± 31
WC-5 (C: 38 at%)	2765 ± 6	2615 ± 86	625 ± 23	661 ± 6
WC-6 (C: 33.4 at%)	2514 ± 2	2478 ± 62	514 ± 54	527 ± 52

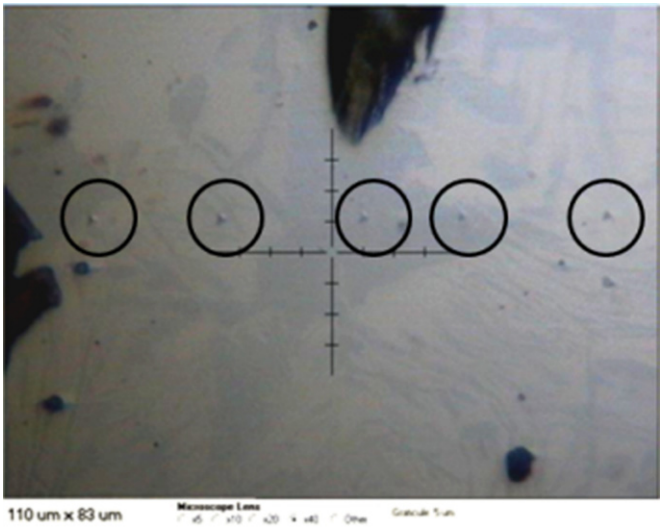

Fig. 9. Micrograph showing nanoindentation marks on WC-4 (40 at% C) sample surface.

exhibit similar trends in this sample. Since nanoindentater mounting was done on single grains, the hardness here indicates local behaviour.

Table 4 presents the global picture in terms of distribution of the white, grey and dark grains in four samples (WC-1, WC-3, WC-5 and WC-6). The WC-5 sample (38 at% C) is seen to contain the highest amount of white grain (70.077%) as against low amounts of grey (28.952%) and dark (0.971%) grains. It is thus found that while locally white grain shows the highest hardness, globally the composite (WC-5 sample) containing the highest amount of white grain also shows the highest hardness. In the overall scenario, microindentation test and nanoindentation test give similar trends in the hardness results of the four composite samples (investigated in the study) even though hardness (VHN) in each method differs in actual observed values.

Young's moduli for the white and the grey grains determined by nanoindentation method are shown in Table 5. The value of the modulus is seen to vary in the range of 514–625 GPa for white grain, 527–754 GPa for grey grain and 30–60 GPa for dark grain. Fairly improved modulus values indicate that some degree of elasticity has

developed in the melt-cast samples, even without heat treatment. Such finding supports the reduced brittle behaviour of the ceramic carbide in the indentation marks (Figs. 7 and 9).

3.5. Raman spectra

Micro Raman spectra of the three typical powder samples (starting tungsten carbide, WC-5 (38 at% C) and WC-7 (30 at% C)) are shown in Fig. 10(A–C) and the peaks have been identified based on the literature. While the starting tungsten carbide shows occurrence of only WC phase in the XRD (Fig. 3A), its SAED pattern (Fig. 5b) shows presence of trace amount of W in addition to WC. Being a metal, W does not show any Raman activity; hence the micro Raman spectra of the starting tungsten carbide powder shown in Fig. 10A is expected to exhibit the spectra due to WC only. The observed Raman peaks, in fact, confirmed the predicted result. Following the work of Mrabet [30], the major peak observed at 801 cm^{-1} is attributed to stretching mode of WC, and the three peaks at 257, 325, 700 cm^{-1} are assigned to incipient oxidation state of WC (indicated in the present paper as WC–O). The

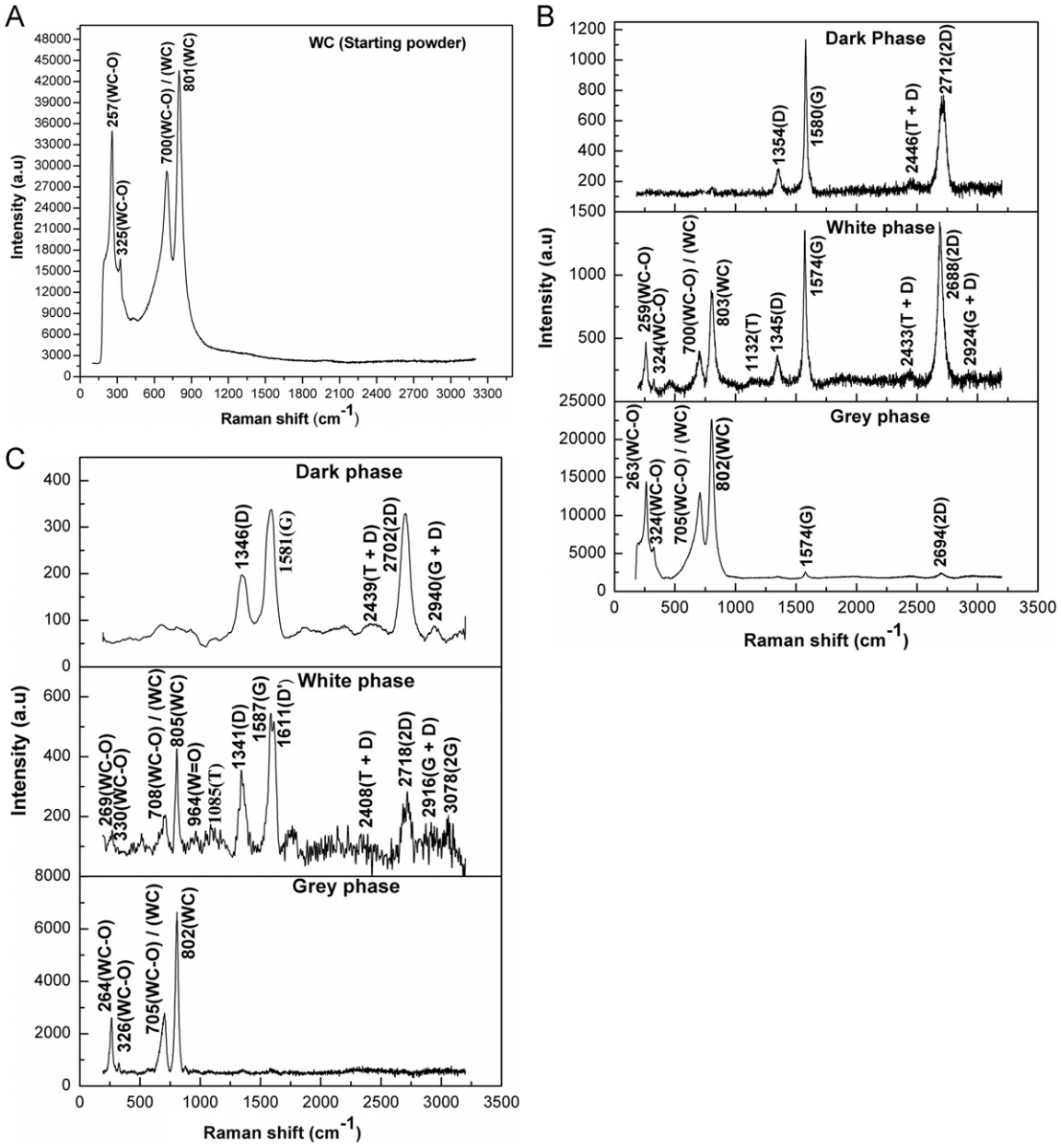

Fig. 10. (A) Raman spectra of the starting tungsten carbide (50 at% C) powder. (B) Raman spectra of arc plasma melt-cast sample WC-5 (38 at% C): G stands for crystalline graphite, D stands for disordered graphite. (C) Raman spectra of arc plasma melt-cast sample WC-7 (30 at% C): G and D indicate as in (B).

peak at 700 cm^{-1} is also attributed to stretching mode of WC [30,31]. In Fig. 10B, the micro Raman spectra have been recorded on the dark, white and grey grains for WC-5 sample (38 at% C, the eutectic composition). Dark grain containing the highest quantity of carbon (Figs. 4f & 6c) which interestingly shows only C peaks due to its various crystallographic phases: 1354 cm^{-1} (D), 1580 cm^{-1} (G) [30–32], 2446 cm^{-1}(T+D) [33], 2712 cm^{-1}(2D) [34]. White grain shows peaks at 259 cm^{-1} (WC–O), 324 cm^{-1} (WC–O), 700 cm^{-1} (WC–O/WC), 803 cm^{-1} (WC), 1345 cm^{-1} (D), 1574 cm^{-1} (G), 2433 cm^{-1} (T+D) and 2688 cm^{-1}(2D) that have been identified following literature [30–34]. Two very small peaks appear here which may be attributed to 1132 cm^{-1} (T) [35] and 2924 cm^{-1} (G+D) [34]. Micro Raman spectra of grey grain presented in Fig. 10(B) show relatively less numbers of peaks as compared to white grain in which intensities of two prominent peaks 1574 cm^{-1}(G) and 2694 cm^{-1}(2D) are significantly reduced. Here, the symbol 2D stands for second order disordered graphite peak, 2G stands for second order graphite peak and T stands for peak due to C–C sp^3 vibration (nanocrystalline diamond) [32,35,36]. Fig. 10C presents the micro Raman spectra observed for the WC-7 sample (30 at% C) having composition below eutectoid range. Compared to WC-5 (38 at% C) sample, an additional peak at 2940 cm^{-1} appears in dark grain of WC-7 sample (30 at% C) which may be attributed to (G+D) [34]. Similarly, three new peaks appear in white grain of this sample (WC-7) which may be attributed as follows: 964 cm^{-1} (W=O) [30], 1611 cm^{-1} (D′) and 3078 cm^{-1} (2G) [33]. Grey grain in this sample shows four peaks similar to that of starting tungsten carbide powder (Fig. 10A). Slight shift in peak position is generally caused by inharmonicity of the molecular vibrations which depend on the method of sample preparation. Table 6 summarises the micro Raman spectra highlighting presence of various phases like WC, C (G, D, D′, 2D) (major); G+D, T, T+D, 2G, 2D of C (minor); and WC–O, W=O (minor) in the melt-cast samples. Taking such results into account along with the results obtained from XRD (Fig. 3(A–D)) and SAED (Figs. 5 and 6b–d), it is evident that W_2C in the composites is not Raman active when incident with 514 nm visible radiation (Ar^+ laser).

4. Conclusion

WC–W_2C composites were prepared for seven different compositions (W:C ratio varying between 70:30 and 50:50) by arc plasma melting and in situ casting. The cast products show recovery/yield in the range of 83.6–91.4 wt%. A relatively higher value of electrical energy consumption varying between 110 and 157 kWh/ kg occurs because of high melting point (~2750 °C) of tungsten carbide and also due to considerable energy loss taking place in the semi-open type plasma furnace employed. XRD analysis of the melt-cast composites shows that WC and W_2C occur as major phases and unbound C mostly grow as minor phases (graphite and diamond/DLC). Lattice constants of WC, W_2C and C (graphite) were determined from XRD and found to closely match with the corresponding values in JCPDS files. FESEM and TEM microstructures reveal three types of grains: white, grey and dark. EDS studies of these grains establish that quantity/amount of carbon in grain decides the appearance or contrast, e.g., in dark grain carbon quantity is the highest; around four times that of white. Evaluation of hardness by micro indentation method shows that microhardness occurs in the range 1684–2080 $VHN_{0.5}$ for white grain, 1604–2055 $VHN_{0.5}$ for grey grain and 516–660 $VHN_{0.5}$ for dark grain. Nanoindentation technique used to measure microhardness on single grains exhibits 31–54% higher hardness for white and grey grains. Marginal superior hardness of white grains over grey ones may be attributed to the presence of diamond/DLC, nanocrystalline diamond and more amounts of W_2C in white grains. Dark grains exhibit hardness, around one third of

Table 6
Raman peak shift (cm^{-1}) and phase assignment in WC (starting powder) and white, grey and dark phases of some typical samples i.e. WC-5 and WC-7.

Peak assignment	Peak position (cm^{-1})						
	WC (starting powder)	WC-5 sample			WC-7 sample		
		Grey phase	White phase	Dark phase	Grey phase	White phase	Dark phase
WC–O	257,325	263,324	259,324	–	264, 326	269, 330	–
WC–O/WC	700	705	700	–	705	708	–
WC	801	802	803	–	802	805	–
W=O	–	–	–	–	–	964	–
T	–	–	1132	–	–	1085	–
D	–	–	1345	1354	–	1341	1346
G	–	1574	1574	1580	–	1587	1581
D′	–	–	–	–	–	1611	–
T+D	–	–	2433	2446	–	2408	2439
2D	–	2694	2688	2712	–	2718	2702
G+D	–	–	2924	–	–	2916	2940
2G	–	–	–	–	–	3078	–

white/grey grains, due to the presence of more amount of carbon in graphite form (major phase). Microhardness is found to be the maximum (for white as well as grey grains) in the case of WC-5 (eutectic composition, 38 at% C) sample. The composite with carbon content slightly below the hypoeutectoid range (i.e. at 30 at% C) shows a sharp rise in microhardness for both white and grey grains. Young's moduli of the melt-cast composites are found in the range 514–625 GPa for white grains and 527–754 GPa for grey grains. Such values for the major phases indicate that the materials are not so brittle like common ceramics. Micro Raman spectral characterisations reveal presence of various phases (major and/or minor) such as WC, carbon (G, D, D′, 2D), carbon (G+D, T, T+D, 2D) and WC-O, W=O in different types of grains including the dark ones. The spectra conclude that W_2C occurring in the WC–W_2C composites is not Raman active when incident with 514 nm visible radiation (Ar^+ laser). In summary, the paper presents a detailed study on the characterisation of arc plasma melt-cast WC–W_2C composites in 30–50 at% C range and correlates microstructural and mechanical properties with carbon composition.

References

[1] Z. Wu, Y. Yang, D. Gu, Q. Li, D. Feng, Z. Chen, Bo. Tu, P.A. Webley, D. Zhao, Silica-templated synthesis of ordered mesoporous tungsten carbide/graphitic carbon composites with nanocrystalline walls and high surface areas via a temperature-programmed carburization route, Small 23 (2009) 2738–2749.

[2] L.E Toth, Transition Metal Carbides and Nitrides, Academic Press, New York, 1971.

[3] G. Jiang, H. Zhuang, W. Li, Combustion synthesis of tungsten carbides under electric field I. Field activated combustion synthesis, Ceramics International 30 (2004) 185–190.

[4] P. Schwartzkopf, R. Kieffer, Refractory Hard Metals Borides, Carbides, Nitrides, and Silicides, The McMillan Co., New York, 1953.

[5] S.T. Oyama (Ed.), The Chemistry of Transition Metal Carbides and Nitrides, Blackie Academic Press, Glasgow, 1995.

[6] H.H. Hwu, J.G. Chen, Surface chemistry of transition metal carbides, Chemical Reviews 105 (2005) 185–212.

[7] S.W.H. Yih, C.T. Wang, Tungsten Sources, Metallurgy and Applications, Plenum Press, New York, 1981, p. 387.

[8] F.A.C. Oliveira, B. Granier, J.M. Badie, J.C. Fernandes, L.G. Rosa, N. Shohoji, Synthesis of tungsten sub-carbide W_2C from graphite/tungsten powder mixtures by eruptive heating in a solar furnace, International Journal of Refractory Metals and Hard Materials 25 (2007) 351–357.

[9] A. Mukhopadhyay, B. Basu, Recent developments on WC-based buck composites, Journal of Materials Science 46 (2011) 571–589.

[10] M. Khechba, F. Hanini, R. Halimi, Study of structural and mechanical properties of tungsten carbides coatings, Nature and Technology. Rev Issue (2011) 09–11 05/June.

[11] E. Zeiler, S. Schwarz, S.M. Rosiwal, R.F Singer, Structural changes of tungsten heating filaments during CVD of diamond, Material Science and Engineering A 335 (2002) 236–245.

[12] I.J. Shon, I.K. Jeong, I.Y. Ko, J.M. Doh, K.D. Woo, Sintering behavior and mechanical properties of WC-10Co, WC-10Ni and WC-10Fe hard materials produced by high-frequency induction heated sintering, Ceramics International 35 (2009) 339–344.

[13] E. Marui, H. Endo, A. Ohira, Wear test of cemented tungsten carbide at high atmospheric temperature (400 °C), Tribology Letters 8 (2000) 139–145.

[14] M. Reyes, A. Neville, Degradation mechanisms of Co-based alloy and WC metal-matrix composites for drilling tolls offshore, Wear 255 (2003) 1143–1156.

[15] H.C. Kim, I.J. Shon, I.Y. Ko, J.K. Yoon, J.M. Doh, G.W. Lee, Fabrication of ultrafine binderless WC and WC-Ni hard materials by a pulsed current activated sintering method, Journal of Ceramic Processing Research 7 (2006) 224–229.

[16] M. Sawan, Radiation shielding requirements for magnets in fusion reactors, Fusion Technology Institute, Univ. Wisconsin, Madison, WI, USA, JAPMED'4, Cairo, Egypt, 17–20 Sept. 2005.

[17] S.W.H. Yih, C.T. Wang, Tungsten Sources, Metallurgy and Applications, Plenum Press, New York, 1981, pp. 392–394.

[18] N. Romanova, P. Chekulaev, V. Dusev, T. Lifshitz, M. Kurdov, Sintered Metal Carbides, Mir Publishers, Moscow, 1972, p. 59.

[19] B.B. Nayak, Enhancement in the microhardness of arc plasma melted tungsten carbide, Journal of Materials Science 38 (2003) 2717–2721.

[20] B.C. Mohanty, S.K. Singh, P.K. Mishra, P.K. Sahoo, S. Adak, Patent no. 1,90,724, Indian, 2003.

[21] A. Sahu, B.B. Nayak, N. Panigrahi, B.S. Acharya, B.C. Mohanty, DC extended arc plasma nitriding of stainless and high carbon steel, Journal of Materials Science 35 (2000) 71–77.

[22] W.C. Oliver, G.M. Pharr, An improved technique for determining hardness and elastic modulus using load and displacement sensing indentation experiments, Journal of Materials Research 7 (1992) 1564–1583.

[23] W. Sabuga, Determination of elastic properties of piston gauges using the strain gauge method, Proceedings of the Seventeenth International Conference. (Force, Mass, Torque and Pressure measurements), IMEKO TC3, Istanbul, Turkey, 17–21 Sept., 2001.

[24] V.Z. Kublii, T.Ya Velikanova, Structural studies of materials: Ordering in the carbide W_2C and phase equilibria in the tungsten-carbon system in the region of its existence, Powder Metallurgy and Metal Ceramics 43 (2004) 630–644.

[25] E. Rudy, Technical Report AFML-TR-69-117, Part V, The phase diagram of W-B-C, Wright-Patterson Air Force Base, Ohio, USA., 1970, p. 6.

[26] V.Z. Kublii, T.Ya. Velikanova, O.A. Gnitetskii, S.I. Makhovitskaya, Structural parameters of the low-temperature matastable form of the carbide W_2C, Powder Metallurgy and Metal Ceramics 39 (2000) 151–156.

[27] L.G. Rosa, P.M. Amaral, C. Anjinho, J.C. Fernandes, N. Shohoji, Fracture toughness of solar-sintered WC with Co additive, Ceramics International 28 (2002) 345–348.

[28] R.L. Orban, Proceedings of the First International Conference on Materials and Manufacturing Technologies (Matehn'94), Cluj-Napoca, Romania, 18–20 May 1994, p. 241.

[29] R.L. Orban, Proceedings of the Fourteenth International Plansee Seminar, Tirol, Austria, 12–16 May 1997, p. 540.

[30] S.E. Mrabet, M.D. Abad, C. López-Cartes, D. Martínez-Martínez, J.C. Sańchez-López, Thermal evoluation of WC/C nanostructured coatings by Raman and in situ XRD analysis, Plasma Processes and Polymers 6 (2009) S444–S449.

[31] F. Porrati, R. Sachser, M. Strauss, I. Andrusenko, T Gorelik, U. Kolb, L. Bayarjargal, B. Winkler, M. Huth, Artificial granularity in two-dimensional arrays of nanodots fabricated by focused-electron-beam-induced deposition, Nanotechnology 21 (2010) 1–7 375302.

[32] V.S. Yadav, D.K Sahu, M. Singh, K. Kumar, Study of Raman spectra of nanocrystalline diamond like carbon (DLC) films composition (sp^2:sp^3) with substrate temperature, Proceedings of the World Congress Engineering and Computer Science (WCECS 2009), ISBN:978-988-17012-6-8, San Francisco, USA, 20–22 Oct. 2009.

[33] E.F. Antunes, A.O. Lobo, E.J. Corat, V.J. Trava-Airoldi, A.A. Martin, C. Veríssimo, Comparative study of first- and

second-order Raman spectra of MWCNT at visible and infrared laser excitation, Carbon 44 (2006) 2202–2211.
[34] H.K. Seo, S.G. Ansari, G.S Kim, Y.S Kim, H.S. Shin, Effect of tungsten/filament on the growth of carbon nanotubes in hot filament chemical vapour deposition system, Journal of Materials Science 39 (2004) 5771–5777.
[35] G. Irmer, A.D. Reisel, Micro-Raman studies on DLC coatings, Advanced Engineering Materials 7 (2005) 694–705.
[36] A.C. Ferrari, Raman spectroscopy of graphene and graphite: Disorder, electron-phonon couping, doping and nonadiabatic effects, Solid State Communications 143 (2007) 47–57.